Mon. Not. R. Astron. Soc. **000**, 1–8 (2016) Printed 13 May 2016 (MN LATEX style file v2.2)

# A self-similar solution for thermal disc winds

C.J. Clarke[1,⋆] and R.D. Alexander[2]
[1] *Institute of Astronomy, Madingley Rd, Cambridge, CB3 0HA, UK*
[2] *Department of Physics & Astronomy, University of Leicester, Leicester, LE1 7RH, UK*

Accepted 2016 May 12. Received 2016 May 9; in original form 2016 March 6

**ABSTRACT**
We derive a self-similar description for the 2D streamline topology and flow structure of an axi-symmetric, thermally driven wind originating from a disc in which the density is a power law function of radius. Our scale-free solution is strictly only valid in the absence of gravity or centrifugal support; comparison with 2D hydrodynamic simulations of winds from Keplerian discs however demonstrates that the scale-free solution is a good approximation also in the outer regions of such discs, and can provide a reasonable description even for launch radii well within the gravitational radius of the flow. Although other authors have considered the flow properties along streamlines whose geometry has been specified in advance, this is the first isothermal calculation in which the flow geometry and variation of flow variables along streamlines is determined self-consistently. It is found that the flow trajectory is very sensitive to the power-law index of radial density variation in the disc: the steeper the density gradient, the stronger is the curvature of streamlines close to the flow base that is required in order to maintain momentum balance perpendicular to the flow. Steeper disc density profiles are also associated with more rapid acceleration, and a faster fall-off of density, with height above the disc plane. The derivation of a set of simple governing equations for the flow structure of thermal winds from the outer regions of power law discs offers the possibility of deriving flow observables without having to resort to hydrodynamical simulation.

**Key words:** accretion, accretion discs:circumstellar matter- planetary systems:protoplanetary discs - stars:pre-main sequence

## 1 INTRODUCTION

Thermally driven disc winds play an important role in the evolution of a variety of astrophysical systems from AGN (Begelman, McKee & Shields 1983) to X-ray binaries (Luketic et al 2010) to protoplanetary discs (e.g. Johnstone, Hollenbach & Bally 1998, Alexander et al 2006, Owen et al 2010). In particular, such winds – where heating is provided by ultraviolet or X-ray radiation from the young star – are widely believed to provide an important mechanism for clearing out proto-planetary discs and thus drawing to a close the epoch of planet formation (see Alexander et al 2014 for a recent review). There is obviously considerable interest in seeking observational diagnostics of such winds (Font et al 2004, Alexander 2008, Gorti & Hollenbach 2008. Hollenbach & Gorti 2009, Ercolano & Owen 2010, Owen et al 2010, Owen et al 2013). These studies are based on numerical radiation-hydrodynamics simulations since – even in the simplest case of an isothermal wind with a prescribed density structure across its base – no *analytic* models for the streamline topology and two dimensional flow structure have been available.

Various authors have attempted to study the structure of thermally driven disc winds. The common approach has been to *assume* a given streamline structure (e.g. Begelman et al 1983, Fukue 1989, Takahara et al 1989, Fukue & Okada 1990, Waters & Proga 2013). In this case, not only is the variation of cross-sectional area along a streamline bundle well defined but so also are the external forces provided by the gravity of the central star and the centrifugal acceleration associated with the flow of angular momentum conserving disc material. In this case, if a barotropic equation of state is assumed, the problem is a variant (with external forces) of the 'de Laval nozzle' flow of compressible fluid along pipes of variable cross-section: there is a unique choice of flow velocity at the base which ensures that the flow makes a transition between subsonic and supersonic flow at its critical point (this latter being defined by a critical relationship between the local streamline divergence and the external forces; Parker 1958). Although such an approach permits a consistent solution *along* each streamline it does *not* ensure a situation of hydrodynamical equilibrium perpendicular to the streamlines. In general such calculations do not consider this issue since they impose a two-dimensional streamline structure. An exception is Fukue & Okada (1990) who constructed a streamline topology for which the components of the external forces (i.e. the gravitational and centrifugal terms) normal to the streamline always

⋆ E-mail: cclarke@ast.cam.ac.uk

cancel. [1]. In fact we will show here that these terms play a minor role in the equilibrium perpendicular to the streamlines even at radii that are well within the 'gravitational radius' (= $GM_*/c_s^2$ for stellar mass $M_*$, sound speed $c_s$) where the depth of the gravitational potential well at the flow base exceeds its thermal energy. This can be broadly understood in that near the flow base the centrifugal and gravitational terms are nearly balanced, whereas at large radii both terms (though unbalanced) become individually small in magnitude. We find that instead the effect that determines the streamline structure over a wide range of launching radii is the balance between the relevant components of the convective derivative of the velocity ($u.\nabla u$) and the pressure gradient. To put it another way, the local *curvature* of the streamlines is jointly determined by the flow velocity and the acceleration provided by pressure gradients normal to the streamlines. At a heuristic level this accounts for the changes in streamline topology as the density profile along the flow base is varied, an effect that is obviously missed by formulations that instead impose the streamline structure *a priori*.

In this paper we present new similarity solutions for isothermal flow from a disc where the density along the flow base is a power law of radius. This similarity solution is valid in the limit of large launching radius where we can neglect external forces (gravity and centrifugal terms) and therefore differs from previously dicussed (magneto-)hydrodynamical self-similar wind solutions which instead impose a constant ratio of sound speed (and Alfven speed) to Keplerian speed at the flow base (e.g. Blandford & Payne 1982, Contopolous & Lovelace 1994, Li 1995, Ostriker 1997, Ferreira & Casse 2004). We are motivated to instead study the globally isothermal case, since this is a reasonable approximation to the results of radiation hydrodynamical modeling of disc photoevaporation from both ionising ultraviolet radiation (Richling & Yorke 1997) and X-rays (Owen et al 2012). Although we might expect that neglect of external forces would result in our similarity solution being valid only at large radii, we will show by comparison with two-dimensional isothermal hydrodynamical simulations that the flow approximately follows the similarity solution down to launching radii as small as $0.5R_g$ (for particular power law choices). Section 2 sets out the derivation of the similarity solution and Section 3 discusses its properties. Section 4 describes the 2D hydrodynamical solutions while Section 5 compares the self-similar solution with the hydrodynamic results both with and without centrifugal/gravitational terms. Section 6 summarises the properties of the solutions and their utility for those modeling the observational consequences of disc winds.

## 2 SIMILARITY SOLUTIONS FOR ZERO-GRAVITY, ISOTHERMAL DISC WINDS

### 2.1 Preliminaries

We consider an axi-symmetric disc wind in the limit of large radius ($R >> R_g = GM/2c_s^2$) and where we thus omit gravitational and centrifugal force terms. In the case that the density at the streamline base is a power law $\rho_b \propto R_b^{-b}$ we see that there are no characteristic length scales associated with the problem. We therefore expect the flow to be self-similar. This means that all streamlines are simply scaled versions of each other and thus (at the same value of $\tilde{s}$, the ratio of the distance along the streamline $s$ to base radius $R_b$) all spatial variables are a given multiple of $R_b$; likewise the density is a given multiple of the density at the streamline base, $\rho_b$, and the velocity is a given multiple of the flow velocity at the flow base ($u_b$). We thus write:

$$u(\tilde{s}, R_b) = u_b \tilde{u}(\tilde{s}) \quad (1)$$

$$\rho(\tilde{s}, R_b) = \rho_b \tilde{\rho}(\tilde{s}) \quad (2)$$

$$R_{eff}(\tilde{s}, R_b) = \tilde{R}_{eff}(\tilde{s}) R_b \quad (3)$$

where $R_{eff}$ is the local radius of curvature of the streamline. In principle the solution that we derive (with gravitational and centrifugal forces omitted) would apply to a purely 2D flow and in what follows we adopt Cartesian coordinates $x$ and $y$ with the flow launched at $x = R_b, y = 0$. Self-similarity then implies

$$y(\tilde{s}, R_b) = \tilde{y}(\tilde{s}) R_b \quad (4)$$

$$x(\tilde{s}, R_b) = \tilde{x}(\tilde{s}) R_b \quad (5)$$

$$r(\tilde{s}, R_b) = \tilde{r}(\tilde{s}) R_b \quad (6)$$

where $r^2 = x^2 + y^2$. When we compare this solution to the case of the disc wind (with gravity and rotation included) $x$ and $y$ can be equated with $R$ and $z$ of a cylindrical coordinate system. We additionally define two angles: $\phi(\tilde{s})$ is the polar angle with respect to the x-axis and $\theta(\tilde{s})$ is the angle between the local streamline tangent and the x-axis. Figure 1 depicts two adjacent streamlines separated by $\Delta R_b$ at the base and thus (given the self-similar geometry), $\Delta r/r = \Delta R_b/R_b$. The area of a streamline bundle normalised to its value at the base is thus given by:

$$\tilde{A} = \tilde{r}^2 \sin(\theta - \phi) \quad (7)$$

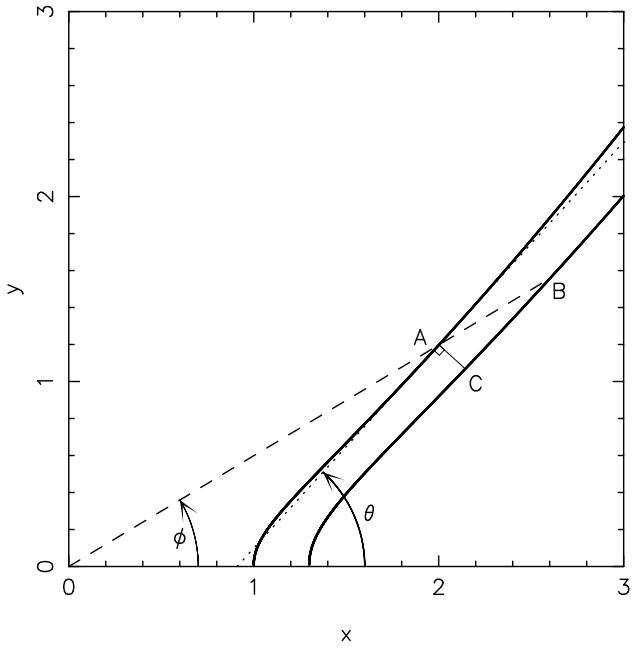


**Figure 1.** Schematic of a pair of scale free streamlines. The component of the pressure gradient normal to the streamline (in direction $\hat{\mathbf{l}}$) is derived from the pressure difference between point C and point A. This can be calculated by considering the pressure difference between A and B (where B is the point on the adjacent streamline with the same value of $\tilde{s}$ as point A) and then considering the pressure difference along the adjacent streamline between points B and C. We define $\phi$ as the polar angle with respect to the $x$-axis, and $\theta$ as the angle between the local streamline tangent (the dotted line) and the $x$-axis.

[1] Icke (1981) adopted a similar approach to deriving the topology of radiatively driven winds.

(assuming that the flow is launched perpendicularly from the $z = 0$ plane: see Section 2.2). We can then write the condition of constant mass flux along the streamline as

$$\tilde{r}^2\tilde{\rho}\tilde{u}\sin(\theta-\phi) = 1 \tag{8}$$

Likewise the invariance of the Bernoulli stream function for an isothermal flow in the absence of gravity or rotation can be written:

$$\tilde{\rho}\exp\left(\frac{u_b^2}{2c_s^2}(\tilde{u}^2-1)\right) = 1 \tag{9}$$

We see immediately from equation (9) that in order for the self-similarity assumption to be valid (i.e. in order that all the scaled quantities are independent of streamline), $u_b$ is independent of streamline.

Normal to the streamlines, force balance between the effect of the pressure gradient perpendicular to the streamline (i.e. in the $\hat{\mathbf{l}}$ direction) and the relevant component of the convective derivative of the velocity gives:

$$\frac{\tilde{u}^2u_b^2}{\tilde{R}_{eff}} = c_s^2\nabla\ln\rho.\hat{l} \tag{10}$$

where we define $R_{eff} > 0$ as implying a geometry that is locally convex upwards (see Appendix).

In order to evaluate the right hand side of equation (10) we need to decompose the change in $\ln\rho$ along $\hat{l}$ into two contributions: the change from streamline to streamline at constant $\tilde{s}$ , i.e., B to A in Figure 1 (which simply relates to the change in $\rho_b$ between the streamlines) and the change from C to B which relates to the gradient in density along a streamline (and which also depends on local streamline geometry). Thus equation (10) becomes

$$\frac{\tilde{u}^2u_b^2}{\tilde{R}_{eff}} = c_s^2\left(\frac{b}{\sin(\theta-\phi)\tilde{r}} + \frac{\partial\ln\rho}{\partial\tilde{s}}\cot(\theta-\phi)\right) \tag{11}$$

Note that the first term dominates near the base of the flow and is positive for an outwardly decreasing density gradient ($b > 0$). The coefficient of the second term is negative and this term dominates in magnitude at large radii where streamlines are nearly radial.

In order to close equations (8),(9) and (11) we need a further relationship between the density gradient along the streamline and the local radius of curvature. We develop this relationship using Cartesian coordinates with independent coordinate $\tilde{y} = y/R_b$ such that the streamline and its local gradient are described in terms of $\tilde{x}(\tilde{y})$, $\tilde{x}'(\tilde{y})$. In Cartesians we can write:

$$\frac{1}{\tilde{R}_{eff}} = \frac{\tilde{x}''}{(1+\tilde{x}'^2)^{1.5}} \tag{12}$$

and can express $\tilde{A}$ (equation (7)) as:

$$\tilde{A} = \frac{\tilde{x}^2 - \tilde{x}\tilde{y}\tilde{x}'}{(1+\tilde{x}'^2)^{0.5}} \tag{13}$$

Then differentiation of (13) wrt $\tilde{y}$ yields:

$$\tilde{x}'' = \frac{(1+\tilde{x}'^2)(\tilde{x}-\tilde{y}\tilde{x}')\tilde{x}'}{\tilde{x}(\tilde{y}+\tilde{x}\tilde{x}')} - \frac{(1+\tilde{x}'^2)^{3/2}\tilde{A}'}{\tilde{x}(\tilde{y}+\tilde{x}\tilde{x}')} \tag{14}$$

Combining (7)-(9) and differentiating with respect to $\tilde{y}$ also yields:

$$\tilde{A}' = \left(\frac{u_b^2}{c_s^2} - \frac{1}{\tilde{u}^2}\right)\tilde{u}'\exp\left(\frac{u_b^2}{2c_s^2}\left(\tilde{u}^2-1\right)\right) \tag{15}$$

Equations (12),(14) and (15) then together allow $\tilde{R}_{eff}$ to be related to $\tilde{u}'$ (for given $\tilde{x}, \tilde{y}, \tilde{x}'$ and $\tilde{u}$). Then using (9) to express the density gradient on the right hand side of equaiton (11) in terms of $\tilde{u}'$ we can convert equation (11) into an equation for $\tilde{u}'$ in terms of $\tilde{x}, \tilde{x}', \tilde{x}''$ and $\tilde{u}$:

$$f(\tilde{x},\tilde{y},\tilde{x}',\tilde{u})\tilde{u}' = g(\tilde{x},\tilde{y},\tilde{x}',\tilde{u}) \tag{16}$$

where

$$f = \frac{-u_b^4\tilde{u}^2}{c_s^2\tilde{x}'(\tilde{x}\tilde{x}'+\tilde{y})}\exp\left(\frac{u_b^2}{2c_s^2}\left(\tilde{u}^2-1\right)\right)\left(1-\frac{c_s^2}{u_b^2\tilde{u}^2}\right)+\frac{\tilde{u}u_b^2(\tilde{x}\tilde{x}'+\tilde{y})}{(1+x'^2)^{1/2}(\tilde{x}-\tilde{y}\tilde{x}')} \tag{17}$$

and

$$g = \frac{bc_s^2(1+\tilde{x}'^2)^{1/2}}{(\tilde{x}-\tilde{y}\tilde{x}')} - \frac{u_b^2\tilde{u}^2\tilde{x}'(\tilde{x}-\tilde{y}\tilde{x}')}{(1+\tilde{x}^2)^{1/2}\tilde{x}(\tilde{x}\tilde{x}'+\tilde{y})} \tag{18}$$

Note that equation (15) is the usual expression for a de Laval nozzle, in which the velocity structure can be computed for known variation of cross-section along the streamline and which shows that a sonic transition is associated with a singular point where the cross-section attains a local extremum. Naturally the streamline solutions that we compute have this property. We however solve (16) instead of (15) and find that for certain ranges of $u_b$, (16) admits solutions that extend to arbitrarily large radii without passing through a critical point. This means that, unlike the case where the variation of cross-section is specified in advance, there is not a *unique* value of the flow velocity at the streamline base which allows the solution to undergo a sonic transition (although there is a range of $u_b$ values for which the flow solution does not extend to infinity with $\tilde{u}\prime$ remaining finite). Within the allowed range of $u_b$, we will find solutions each of which has a different variation of $\tilde{A}$ along the streamline (and a different topology), the geometrical properties of the flow self-adjusting so as to maintain momentum balance perpendicular to the streamlines.

### 2.2 Method of solution

We start by adopting a trial value of $u_b$ and construct the streamline from its base ($\tilde{s} = 0$, $\tilde{r} = 1$, $\phi = 0$, $\theta = \pi/2$). We assume that the flow leaves the disc perpendicularly (in order to compare directly with numerical simulations that make this assumption; e.g., Font et al 2004, and the simulations presented in Sections 4 & 5)). We solve for the streamline structure as an initial value problem, choosing $\tilde{y}$ as the independent variable that is advanced along the streamline. At any point, P, on the streamline, at which we know the current values of $\tilde{x}, \tilde{y}, \tilde{u}$ and $\tilde{x}'$, we use equation (16) to evaluate $\tilde{u}'$; advancing $\tilde{y}$ by $\Delta\tilde{y}$ we then calculate the value of $\tilde{u}$ at the next position along the streamline, P', using a first order Euler method (verifying that the resulting solutions are independent of $\Delta\tilde{y}$). Equations (14) and (15) are then used to calculate $\tilde{x}''$ at P. The $\tilde{x}$ coordinate of P' and local streamline gradient $\tilde{x}'$ are then readily determined:

$$\tilde{x}|_{P'} = \tilde{x}|_P + \tilde{x}'|_P + \Delta\tilde{y} + 0.5\tilde{x}''|_P\Delta\tilde{y}^2 \tag{19}$$

$$\tilde{x}'|_{P'} = \tilde{x}'|_P + \tilde{x}''|_P\Delta\tilde{y} \tag{20}$$

The streamline geometry and flow velocity are now known at point P', and the solution is then integrated to the next streamline point.

## 3 RESULTS

### 3.1 General properties of the flow

We consider solutions for which $\tilde{x} = 1, \tilde{y} = 0$ and $\tilde{x}' = 0$ at the flow base. In this case the corresponding values of $f$ and $g$ at the flow base are:

**Table 1.** Self-similar streamline properties. Columns (1): index of power law for base density. (2): Maximum value of Mach number at launch such that solution accelerates monotonically to large radius. The following properties correspond to the streamline solution at this maximum launch Mach number: (3) and (4) are normalised coordinates of the sonic point, (5) is the normalised flow velocity at a height of 5× the initial launch radius above the disc plane and (6) is the angle between streamline and x-axis at this location.

| b | $u_b/c_s$ | $\tilde{x}_{sonic}$ | $\tilde{y}_{sonic}$ | $\tilde{u}/c_s\|_{\tilde{y}=5}$ | $\theta\|_{\tilde{y}=5}$ |
|---|---|---|---|---|---|
| 0.5 | 0.92 | 1.02 | 0.30 | 1.92 | 81 deg |
| 0.75 | 0.85 | 1.06 | 0.33 | 2.02 | 72 deg |
| 1 | 0.77 | 1.09 | 0.35 | 2.35 | 76 deg |
| 1.5 | 0.56 | 1.17 | 0.30 | 2.71 | 57 deg |
| 2 | 0.29 | 1.23 | 0.16 | 3.28 | 38 deg |

$$f = u_b^2\left(\frac{u_b^2}{c_s^2}\right) \tag{21}$$

and

$$g = bc_s^2 \tag{22}$$

so that for sub-sonic launch velocities $f$ and $g$ are both $> 0$ and thus $\tilde{u}' > 0$ (i.e. the flow accelerates). Both terms contributing to $f$ remain $> 0$ while the flow remains subsonic and we also find that $g$ remains positive. Consequently the flow accelerates monotonically to the sonic point. At large radius, the flow becomes increasingly radial [i.e. $(1 - \tilde{y}\tilde{x}'/\tilde{x})$ tends to 0] so that the second term in $g$ can be neglected and the limiting form of $g$ is

$$g = \frac{bc_s^2(1+\tilde{x}'^2)^{1/2}}{(\tilde{x} - \tilde{y}\tilde{x}')} \tag{23}$$

The limiting form of $f$ is:

$$f = \frac{u_b^2\left(1 - \frac{u_b^2\tilde{u}^2}{c_s^2}\right)\exp\left(\frac{u_b^2}{2c_s^2}(\tilde{u}^2-1)\right)}{\tilde{x}'(\tilde{x}\tilde{x}' + \tilde{y}')(\tilde{x} - \tilde{y}\tilde{x}')} + \frac{\tilde{u}u_b^2(\tilde{x}\tilde{x}' + \tilde{y})}{(\tilde{x} - \tilde{y}\tilde{x}')(1+\tilde{x}'^2)^{1/2}} \tag{24}$$

The first term in $f$ is negative in the supersonic regime whereas $g$ and the second term in $f$ are both positive. Thus, depending on the value of $u_b$ and the resulting streamline topology, the two terms in $f$ may or may not cancel at finite $\tilde{x}$. If they do *not*, then $\tilde{u}'$ (equation 16) remains finite and positive at all $\tilde{x}$ (i.e. the flow accelerates monotonically to arbitrarily large velocity). However, if the first term in $f$ ever becomes greater or equal in magnitude to the second term, then $\tilde{u}'$ becomes infinite and changes sign. We are here concerned with the former class of solution as representing a physical flow to infinity and we thus require that $f$ always remains positive. We cannot impose this as an analytic condition without solving for the streamline topology. We nevertheless see that because the (negative) magnitude of the first term of f is an increasing function of $u_b$, we expect that physical solutions that reach infinity are those with relatively low $u_b$. We will find below that this is indeed the case: for each value of $b$ we are able to attain a range of flow solutions corresponding to a range of $u_b$ values up to a maximum value $u_b = u_{b_{max}}(b)$. We will go on to show in Section 5 that time-dependent hydrodynamical sumulations in fact tend to the flow solutions with $u_b = u_{b_{max}}(b)$.

### 3.2 Flow solutions as a function of b

We detail the properties of the streamline solution as a function of $b$ in Table 1, in each case using the solution for which the Mach number has the maximum value for which $f$ (equation (24)) remains positive (and hence $\tilde{u}$ increases monotonically along the streamline). We plot the corresponding self-similar streamline geometries (as derived in Section 2) as the red curves in Figure 2. It is immediately obvious that the flow geometry is a sensitive function of $b$, with much more vertical trajectories being associated with lower values of $b$. This result can be readily understood inasmuch as the value of $b$ controls the acceleration experienced perpendicular to the streamline; for larger values of $b$, momentum balance is achieved by the streamline adopting a smaller radius of curvature (equation (12)). The maximum value of flow launch velocity also varies systematically with $b$, but more mildly, so that the mass flux for given local base density is reduced by about a factor two going from $b = 0.5$ to $b = 1.5$.

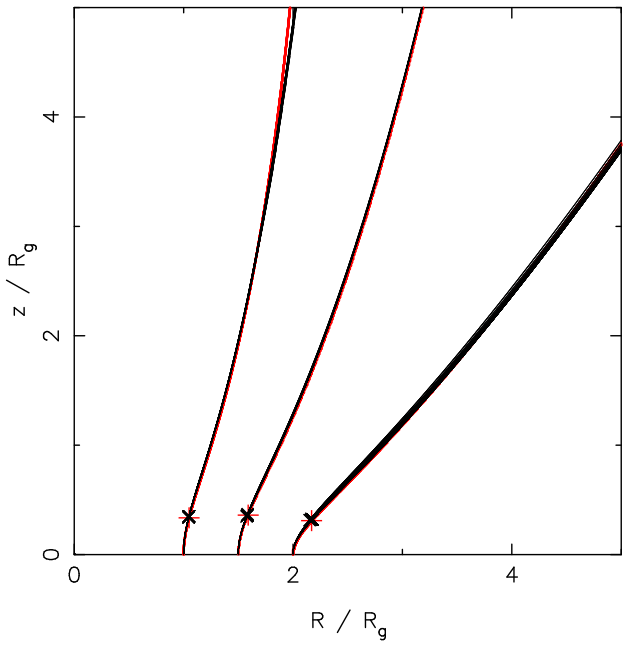


**Figure 2.** Streamline topology for $b = 0.75$, $b = 1.$ and $b = 1.5$ (left to right): self-similar solution (red) and scale free hydrodynamical simulation (black) for streamlines originating at $R = 1$ (for clarity, the latter two streamlines are each laterally displaced by 0.5 while preserving the relative scale on the two axes). A series of different (re-scaled) streamlines are plotted for each hydrodynamical simulation, showing that the simulations are indeed scale-free (though slight departures from self-similarity are visible for $b = 1.5$). For each streamline the sonic point is plotted as either a red "plus" ( self-similar solution) or a black cross (hydrodynamical simulations).

## 4 2D HYDRODYNAMICAL SIMULATIONS: METHOD

In order to test our self-similar solution we have run a series of numerical hydrodynamical calculations for comparison. We use the ZEUS2D hydrodynamics code (Stone & Norman 1992), parallelised (for a shared-memory architecture) using the OpenMP formalism[2], and adopt the same numerical approach previously used by Font et al (2004) and Alexander (2008). We assume azimuthal and midplane symmetry, as in the self-similar solution, and use a polar $[(r, \theta)]$ grid spanning $\theta = [0, \pi/2]$. The (fixed) grid is logarithmically spaced in $r$ and linearly spaced in $\theta$, so that the grid

[2] See `http://openmp.org`

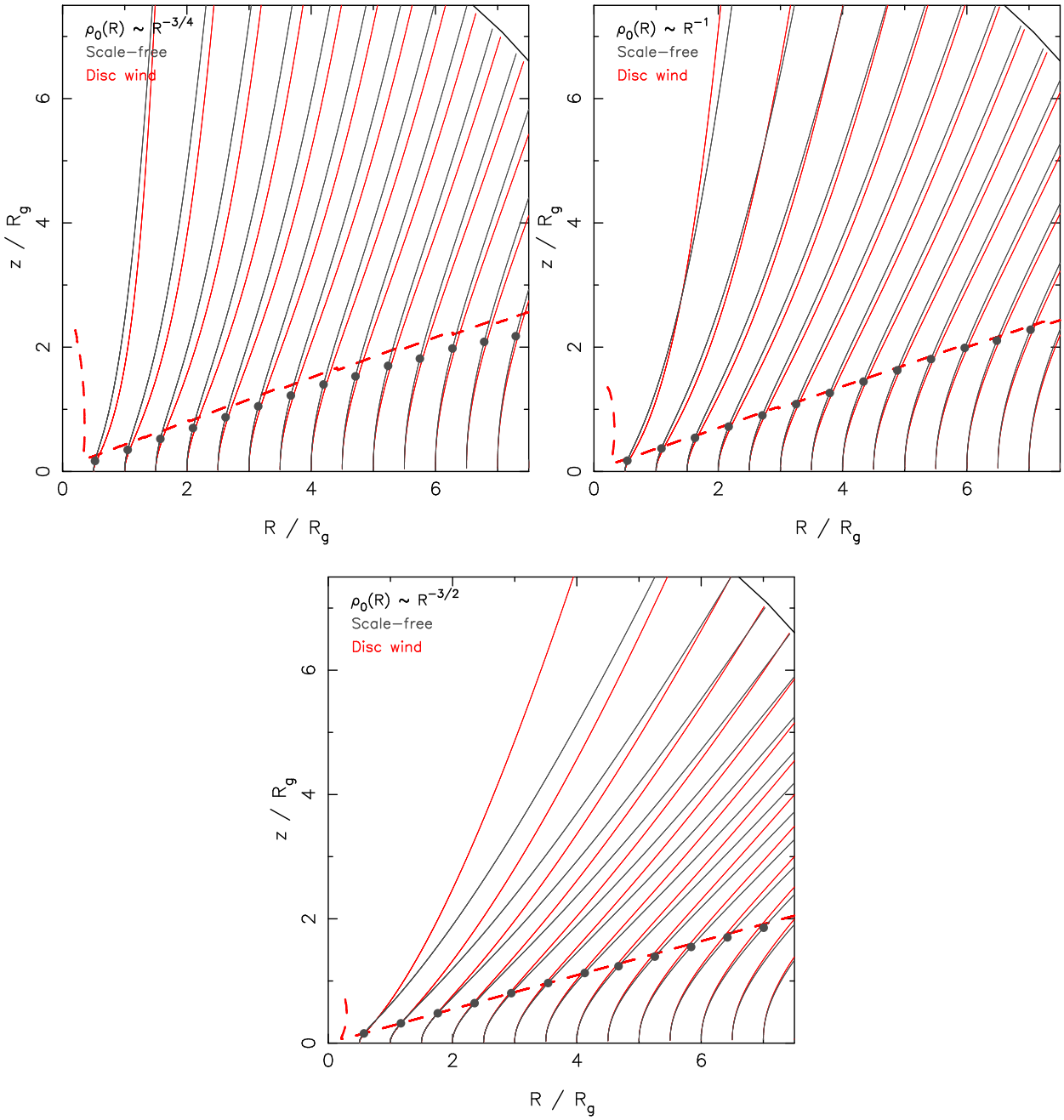


**Figure 3.** Comparison between the scale free (grey) and disc wind solutions (red) for $b = 0.75$, $b = 1$ and $b = 1.5$. The solid lines show streamlines originating from $R = 0.5R_g$, $1.0R_g \ldots 7.0R_g$. The sonic surfaces in the disc wind simulations are plotted as dashed red lines, while the corresponding sonic points along the scale-free streamlines are denoted by grey circles. The solid black lines denote the boundaries of the computational grid.

cells are approximately square throughout (i.e., $\Delta r = r\Delta\theta$). The grid has $N_\theta = 200$ cells in the polar direction and spans the range $r = [0.01R_g, 10.0R_g]$, and therefore $N_r = 883$ cells in the radial direction. We adopt the standard second-order (van Leer) interpolation scheme, and the von Neumann & Richtmyer artificial viscosity (with $q_{\rm visc} = 2.0$). The gas has an isothermal equation of state ($P = c_s^2\rho$), and we adopt outflow boundary conditions at both the inner and outer radial boundaries. At the upper polar boundary (the $z$-axis) we adopt a reflective boundary condition, but little or no material reaches this boundary so this has no influence on the flow solutions. At the lower polar boundary ($z = 0$) we impose a power-law density profile

$$\rho_0(R) = \rho_g \left(\frac{R}{R_g}\right)^{-b} \tag{25}$$

and set the radial velocity $v_r(R) = 0$ in the boundary cells. The polar velocity out of the base cells is not prescribed, but rather computed self-consistently by the hydrodynamic code. We work in dimensionless units: the unit of length is $R_g$; the unit of time is the orbital period at $R_g$; and the density is normalised such that $\rho_g = 1$. Each model rapidly evolves towards a steady state. We run each simulation for $t = 50$ time units and, to minimise numerical noise, take the average density and velocity fields over $t = [40, 50]$ as the

final flow solution. All simulations were run on the ALICE[3] and DiRAC2/*Complexity*[4] high-performance computing clusters at the University of Leicester.

We run two sets of models: i) disc wind models; and ii) scale-free models. In the disc wind models the rotation option in ZEUS2D is turned on, introducing a rotational (centrifugal) pseudo-force. We include gravitational accelerations due to a point mass (of mass $M_*$) at the origin, and the base cells are given Keplerian velocities in the orbital direction. In the scale-free models both centrifugal and gravitational accelerations are turned off; these runs should therefore exactly match the self-similar solutions .

## 5 2D HYDRODYNAMICAL SIMULATIONS: COMPARISON WITH SELF-SIMILAR SOLUTIONS

### 5.1 Comparison between self-similar solution and scale-free hydrodynamical simulations

The purpose of the scale-free models is to test our numerical method against the self-similar solution. Figure 2 demonstrates that there is almost perfect agreement between the self-similar solution (red) and scale-free hydrodynamic models (black) for three values of $b$ between 0.75 and 1.5. For each hydrodynamic simulation we plot a series of re-scaled streamlines originating from different values of $R$. In each case the sonic point is found to lie within one grid cell of its position in the self-similar solution, and the excellent agreement between streamlines originating from different radii indicates that the numerical calculations are indeed scale-free. However, some small departures from self-similarity are visible in Figure 2 (particularly for $b = 1.5$). These are due to the boundary conditions (which are by construction not scale-free) and other numerical effects, which we detail below.

The boundary conditions introduce two different numerical artefacts. First, the standard ZEUS "outflow" boundary condition is exact only for supersonic flow along grid-lines (i.e., perpendicular to the boundary; Stone & Norman 1992). As the flow is not purely radial, we invariably see some spurious reflection from the radial boundaries. This primarily occurs at the outer boundary, and is most prominent in the simulations with smaller values of $b$ (where the tangential velocity at the boundary is largest). This effect is most visible in Fig. 4, where we see that the otherwise-constant launch velocity in the scale-free simulations increases progressively for $R/R_{\rm g} \gtrsim 8$. Test calculations with a larger outer grid radius ($R/R_{\rm g} = 20$) confirm that this is indeed a boundary effect, which alters the flow solution in the outer ∼20% of the computational domain (see also discussion in Alexander et al. 2006).

A second artefact arises because the imposed base density profiles imply a radial pressure gradient for $b \neq 0$, and are therefore not strictly consistent with the $v_r = 0$ midplane boundary condition. This effect is small in the scale-free simulations (and negligible in the disc wind simulations), but becomes more pronounced for larger values of $b$ and is the origin of the small departures from self-similarity seen in Fig. 2 for $b = 1.5$. Values of $b \gtrsim 2$ result in simulations that show significant departures from self-similarity.

Finally, in the scale-free simulations (only) the required numerical resolution is not independent of $b$. Smaller values of $b$ result in higher launch velocities, and the launch velocity approaches the sound speed for $b \lesssim 0.5$. In such cases the sonic transition is poorly resolved, with the sonic point found only a few grid cells along each streamline. For $b \gtrsim 0.6$ our calculations are well resolved, but for lower values of $b$ the sonic point is very close to the base of the flow, and the resolution required to achieve numerical convergence is prohibitively expensive. Given these numerical limitations, we restrict our hydrodynamic simulations to the range $b = 0.75$–$1.5$[5]

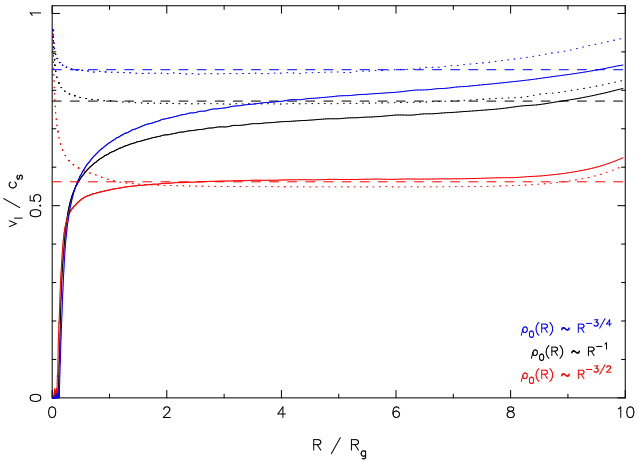


**Figure 4.** The launch velocity at the flow base as a function of streamline radius for the self-similar solution (dashed), scale free hydrodynamical simulation (dotted) and disc wind solutions (solid) for $b = 0.75$ (blue), $b = 1$ (black) and $b = 1.5$ (red). The mild deviation of the scale free hydrodynamical solution from constant launch velocity near the boundaries is a numerical artefact. The rough constancy of the launch velocity for the disc wind solution over a large dynamic range demonstrates the applicability of the scale free approximation in these cases.

### 5.2 Comparison between the scale-free/ self-similar solutions and the disc wind simulations.

The disc wind models differ from those discussed above in that they include rotation and gravitational acceleration by the central star. We expect such models to approach the scale-free results in the limit of large $R/R_g$, but here investigate the region over which the scale-free results are approximately applicable to real disc winds. We focus our comparisons on the streamline topology, as this uniquely determines both the launch velocity and (as the base density is fixed) the mass-loss profile. Figure 3 compares the disc wind streamlines and sonic surfaces with the scale free trajectories for $b$ in the range 0.75 to 1.5. We depict streamlines with base radii in the range $0.5R_g$ to $7.5R_g$. Note that whereas in the presence of gravity and rotation, the wind velocity drops steeply at small radii (so that there is an 'inner most streamline' at $\sim 0.2R_g$; Font et al 2004), the scale free simulations naturally extend to arbitrarily small radii. For the power law profiles considered here, the total mass loss rate still converges at small radius but we caution that the scale free solutions may over-estimate the signature generated by high density wind tracers at small radii.

Quantitatively, the self-similar solution places the sonic point very close to its true location for streamlines originating at $R \gtrsim R_g$. In terms of the distance along each streamline, for $b = 1.5$ we find

[3] See `http://go.le.ac.uk/alice`
[4] See `http://www.dirac.ac.uk`

[5] Note in the disc wind runs the flow is accelerated over a length-scale $\sim R_{\rm g}$, which is always well resolved in our simulations. The lack of numerical convergence for small values of $b$ only occurs in the scale-free simulations.

that the sonic point in the scale-free solution is within ±3% of its location in the disc wind simulations for $R > R_g$, and is only 6.5% in error even for the streamline originating at $0.5R_g$. For $b = 1.0$ the self-similar solution under-estimates the distance to the sonic point by ≃5% over most of the computational domain, but this rises to 13% for the streamline originating at $R_g$, and 26% at $0.5R_g$. The solution for $b = 0.75$ shows the least good fit with the disc wind model, but even then the agreement is very encouraging: the distance to the sonic point is within 15% of the correct value over most of the domain, but is too small by 30% at $R_g$ and 43% at $0.5R_g$. As an additional test we also compute (integrated) mass-loss rates over the range $[0.5R_g, 5R_g]$. As expected the scale-free solution over-estimates the mass-loss at small radii, but the agreement is still remarkably good: the ratios between the self-similar mass-loss rates and those in the disc wind simulation are 1.02, 1.13 and 1.16, for $b = 1.5$, 1.0 & 0.75 respectively.

In general, the agreement between disc wind simulations and the scale free solution improves at larger values of $R/R_g$ as expected. Nevertheless the degree of agreement varies with $b$ in a way that can be simply understood in terms of the curvature of the streamlines in the scale free solutions. In the scale free case, the local streamline curvature is set by equation (10) which balances the component of the pressure force normal to the streamline with the convective derivative of the velocity. The solution will thus be approximately scale free in cases where the component of gravitational acceleration normal to the streamline is much less than the convective derivative, i.e. $u^2/R_{eff} >> GM/R^2$. Given that the flow velocity is of order $c_s$, this condition becomes $(R/R_g) \times (R/R_{eff}) >> 1$. Inspection of Figure 3 confirms this condition. In regions where the scale free solution has a small radius of curvature ($R_{eff} \leqslant R$), the scale free solutions provide a good match to the full disc wind solutions even at relatively low values of $R/R_g$. This is particularly evident in the case $b = 1$ and also near the flow base in the case $b = 1.5$. The agreement in the case $b = 1$, even at base radius as low as $R_b = 0.5R_g$ is striking. The disc wind solutions however deviate more strongly from the scale free solutions in regimes where the streamlines are nearly straight (i.e. large $R_{eff}$). Such mild curvature is seen in the streamlines for the $b = 0.75$ case, even at the flow base, as a result of the relatively weak pressure gradient in this case. Mild curvature in the scale free solution is also seen at larger heights in the $b = 1.5$ case. This contrasts with the $b = 1$ case where the component of the pressure gradient normal to the streamlines changes sign over a short distance around $z/R_B \sim 1$: at larger heights the streamlines are concave upwards because the pressure declines with increasing height. For $b = 1.5$, by contrast, the pressure gradient at large heights is small in magnitude and the streamlines are almost straight. In all cases where the scale free solution yields solutions with mild curvature, the addition of gravity modifies the streamlines, yielding solutions that are concave upwards.

In summary, the scale free solutions do a remarkably good job at approximating the disc wind solutions for $b = 1$ and $b = 1.5$ although there is some deviation in the latter case for base radii within a few times $R_g$. Even this latter deviation is however only apparent at heights $z > R_b$; the good agreement near the flow base means that the launch velocities are independent of streamline (as in the scale free solution) even for $R/R_g$ as low as 1 (see Figure 4). In the case of $b = 0.75$, by contrast, the scale free solution exhibits mild curvature throughout and thus gravity plays an important role in setting the streamline topology even at $R/R_g$ as large as 10. This is also demonstrated by Figure 4, which shows that for $b = 0.75$ the disc wind solutions never attain the limit of constant launch velocity (as required by a scale-free solution) within the computational grid ($R/R_g < 10$).

## 6 CONCLUSIONS

We have developed a similarity solution for the structure of an isothermal disc wind with a power law base density profile ($\rho \propto R_b^{-b}$). The problem is strictly scale free only in the case that both rotation and gravity are neglected; we have verified that the solutions obtained are in excellent agreement with hydrodynamic simulations in this case and that the streamline shape becomes progressively more vertical as $b$ (the index of the base density power law) is reduced. The results can be simply understood in terms of the force balance perpendicular to the streamlines which implies that streamlines become more curved for steeper density profiles (see Figure 2).

We have also compared these solutions with disc wind simulations which also include Keplerian rotation and the gravity of the central object. We find that the self-similar solution provides a good match to the disc wind simulations over a wide range of radii. This agreement is particularly good in the case of the steeper profiles ($b = 1$ and $b = 1.5$, which are more appropriate to those expected in photoevaporating winds; Font et al 2004). In the case $b = 1$ this excellent agreement extends in to streamlines originating from a factor two within $R_g$ (see Figure 3).

The self-similar solution derived here will be useful for the modelling of disc winds without recourse to hydrodynamic simulations. There are numerous potential applications in terms of modeling the line profiles and free-free emission from thermally driven disc winds, particularly in the protoplanetary disc context. Such solutions also provide a useful tool for benchmarking simulations involving the entrainment of dust by disc winds (cf Hutchison & Laibe 2016).

## ACKNOWLEDGMENTS

We thank James Owen for useful discussions and the referee for comments that have helped to improve the paper's clarity. This work has been partially supported by the DISCSIM project, grant agreement 341137 funded by the European Research Council under ERC-2013-ADG. RDA acknowledges support from STFC through an Advanced Fellowship (ST/G00711X/1), and from the Leverhulme Trust through a Philip Leverhulme Prize. Astrophysical research at the University of Leicester is supported by an STFC Consolidated Grant (ST/K001000/1). This research used the ALICE High Performance Computing Facility at the University of Leicester. Some resources on ALICE form part of the DiRAC Facility jointly funded by STFC and the Large Facilities Capital Fund of BIS. This work also used the DiRAC *Complexity* system, operated by the University of Leicester IT Services, which forms part of the STFC DiRAC HPC Facility (`http://www.dirac.ac.uk`). This equipment is funded by BIS National E-Infrastructure capital grant ST/K000373/1 and STFC DiRAC Operations grant ST/K0003259/1. DiRAC is part of the UK National E-Infrastructure.

## REFERENCES

Alexander, R., 2008. MNRAS 391,L64
Alexander, R., Armitage, P., 2009. ApJ 704,989

Alexander, R., Clarke, C., Pringle, J., 2006. MNRAS 369,216
Alexander, R., Pascucci, I., 2012 MNRAS 422, L82
Alexander R., Pascucci I., Andrews S., Armitage P., Cieza L., Protostars and Planets VI. Beuther H., Dullemond C. P., Klessen R. S., Henning T. K., editors. Tuscan, AZ: Univ. Arizona Press; 2014. p. 475.
Begelman, M., McKee, C., Shields, G., 1983. ApJ 271,70
Blandford, R., Payne, D, 1982. MNRAS 199,883
Contopoulos, J., Lovelace, R., 1994. ApJ 429,139
Ercolano, B., Owen, J., 2010. MNRAS 406,1553
Ferreira, J., Casse, F., 2004. ApSS 292,479
Font, A., McCarthy. I., Johnstone, D., Ballantyne, D., 2004. ApJ 607,890
Fukue, J., 1989. Pub. ASJ 41,123
Fukue, J., Okada, R., 1990. Pub. ASJ 42,249
Gorti, U., Hollenbach, D., 2009. ApJ 690,1539
Hollenbach, D., Gorti, U., 2009. ApJ 703,1203
Hutchison, M., Laibe, G., PASA in press, arXiv: 1602.06044v1
Icke, V., 1981. ApJ 247,152
Johnstone, D., Hollenbach, D., Bally, J., 1998. ApJ 499,758
Luketic, S., Proga, D., Kallman, T., Raymond, J., Miller, J., 2010. ApJ 719,515
Ostriker, E., 1997. ApJ 486,291
Owen, J., Ercolano, B., Clarke, C., Alexander, R., 2010. MNRAS 401,1415
Owen, J., Clarke, C., Ercolano, B., 2012. MNRAS 422,1880
Owen, J., Scaife, A., Ercolano, B., 2013. MNRAS 434,3378
Parker, E., 1958. ApJ 128,664
Richling, S., Yorke, H., 1997. A & A 327,317
Stone J. M., Norman M. L., 1992, ApJS, 80, 753
Takahara, F., Rosser, R., Kusnose, M., 1989. ApJ 346,122
Waters, T., Proga, D., 2012. MNRAS 426,2239

## 7 APPENDIX: DERIVATION OF THE CONVECTIVE DERIVATIVE

The streamline geometry is set by a requirement of hydrodynamic force balance perpendicular to the flow streamlines wherein the component of the acceleration due to the pressure gradient in this direction is matched by the corresponding component of the convective derivative, $u.\nabla u$. As in the main text, we denote unit vectors perpendicular and parallel to the streamline by $\hat{l}$ and $\hat{s}$ respectively. Here we will show that $(u.\nabla u).\hat{l} = -u^2/R_{eff}$ (see equation 10) where $R_{eff}$ is the local radius of curvature of the streamline such that $R_{eff} > 0$ implies that the streamline is convex upwards (i.e. in the direection of increasing $l$).

We consider a 2D coordinate system s,l where $l$ is the perpendicular distance of any point P from a fixed (reference) streamline which passes through point O (coordinates 0,0) and where $s$ is the distance measured along the reference streamline between point O and the point on the streamline whose normal passes through P. Consider now points A and B with coordinates 0,l and ds, l+dl. If the radius of curvature of the streamline at 0 is $R_{eff}$ then the distance between points A and B can be written:

$$AB^2 = dl^2 + \left(\frac{R_{eff}+l}{R_{eff}}\right)^2 ds^2 \tag{26}$$

The components of the metric tensor in this coordinate system are thus $g_{ll} = 1$ and $g_{ss} = \left(\frac{R_{eff}+l}{R_{eff}}\right)^2$.

The definition of the convective derivative with respect to arbitrary coordinates $q_i$ is given (e.g. http://mathworld.wolfram.com/ConvectiveOperator.html) by

$$[u.\nabla u]_j = \Sigma_{k=1}^{k=2}\left(\frac{u_k}{h_k}\frac{\partial u_j}{\partial q_k} + \frac{u_k}{h_k h_j}\left(u_j\frac{\partial h_j}{\partial q_k} - u_k\frac{\partial h_k}{\partial q_j}\right)\right) \tag{27}$$

where $h_i^2 = g_{ii}$.

Since the coordinate $s$ lies along the streamline direction, we have $u_s = u$ and $u_l = 0$; this implies:

$$[u.\nabla u]_l = -\frac{u}{h_s h_l}u\frac{\partial h_s}{\partial l} \tag{28}$$

i.e.

$$[u.\nabla u]_l = -u^2\frac{\partial \ln h_s}{\partial l} \tag{29}$$

Since [6]

$$\frac{\partial \ln h_s}{\partial l} = \frac{1}{R_{eff}+l} \tag{30}$$

then at point O ($l = 0$), this is simply $1/R_{eff}$. Thus

$$[u.\nabla u]_l = -\frac{u^2}{R_{eff}} \tag{31}$$

[6] Note that in deriving the identity equation (31) we are considering the component of $u.\nabla u$ at an arbitary point O and define a coordinate system based on the streamline passing through O with a particular value of $R_{eff}$. For this derivation, $R_{eff}$ is then a *fixed* property of the coordinate system and is not a function of $l$. The derived identity is then valid at all points, regardless of whether, in a given velocity field, $R_{eff}$ varies between streamlines.